Design of Broadband Sub-Wavelength Grating Couplers with Low Back Reflection

YUN WANG[1*], WEI SHI[2], XU WANG[3], ZEQIN LU[1], MICHAEL CAVERLEY[1], RICHARD BOJKO[4], LUKAS CHROSTOWSKI[1], AND NICOLAS A. F. JAEGER[1]

[1] Department of Electrical and Computer Engineering, University of British Columbia, Vancouver, BC, Canada
[2] Department of Electrical and Computer Engineering, Université Laval, QC, Canada
[3] Lumerical Solutions, Vancouver, BC, Canada
[4] Department of Electrical Engineering, University of Washington, Campus Box 352500, Seattle, Washington 98195, USA
[*] Corresponding author: yunw@ece.ubc.ca

Compiled September 8, 2015

We present a methodology to design broadband grating couplers using one dimensional sub-wavelength gratings. Using the presented method, we design sub-wavelength grating couplers (SWGCs) with 1-dB bandwidths ranging from 50 nm to 90 nm. Our designed SWGCs have competitive coupling efficiency, as high as -3.8 dB for the fundamental TE mode, and state-of-the-art back reflections, as low as -23 dB.

OCIS codes: *(050.2770) Gratings; (050.2065) Effective medium theory; (050.6624) Subwavelength structures.*

http://dx.doi.org/10.1364/ao.XX.XXXXXX

The silicon-on-insulator (SOI) platform, with a high index contrast between the silicon layer and its cladding, provides an unprecedented opportunity to make highly integrated photonic circuits with sub-micron silicon-wire waveguides [1]. However, the small feature sizes of the waveguides raise the problem of large mode mismatch when coupling light from optical fibers to the sub-micron silicon waveguide cores. Tapered edge couplers [2] and surface grating couplers [3] are two popular devices used to efficiently couple light between optical fibers and sub-micron silicon waveguides. Compared to the edge couplers, grating couplers have the advantages of lower cost, easy alignment, compact shape, *etc*. Grating couplers also enable wafer-scale automated measurement, without the need to dice the wafer. One of the major drawbacks of grating couplers are their narrow bandwidths. Significant effort has been devoted to improve the coupling efficiency of grating couplers [4–11], while only a few attempts have been made to improve the bandwidths [12–16]. Thorough bandwidth analyses of grating couplers have been presented in [12, 14], where the bandwidth of a grating coupler was attributed to the mismatch of the effective indices between the diffracted beam and the actual grating structure. Alternatively [13], the bandwidth of a grating coupler can be attributed to the wavelength dependent diffraction angle of the grating coupler. Sub-wavelength gratings have been used to improve the bandwidths of grating couplers [13, 15, 16]. Compared to two dimensional sub-wavelength gratings, one dimensional sub-wavelength gratings have the advantages [11] of lower fabrication cost, higher fabrication accuracy and repeatability, design simplicity, *etc*.

In this letter, we demonstrate broadband sub-wavelength grating couplers (SWGCs) using one dimensional sub-wavelength gratings. A schematic of the cross-section of an SWGC is shown in Fig. 1(a). The operating wavelength, λ, is shown in the same figure for comparison purposes. Our design methodology follows a four-step process. In the first step, we derive an expression for the 1-dB bandwidth of a grating coupler, that depends on the group index and the incident angle. Based on the derived expression, a specific incident angle is chosen for further design optimization. Then three more steps are followed to finalize various design parameters using the particle swarm algorithm (PSA) [17] and effective medium theory (EMT) [18].

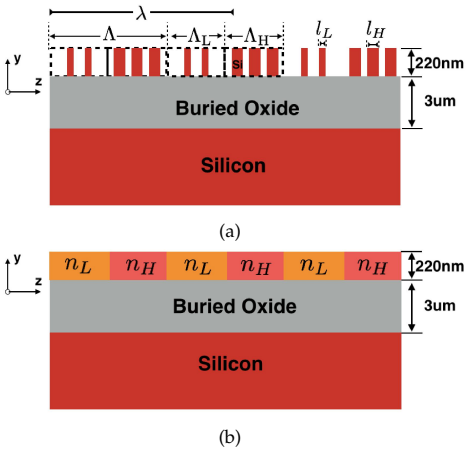

Fig. 1. (a) Schematic of the cross-section of an SWGC with one-dimensional sub-wavelength gratings; (b) schematic of an SWGC with refractive index regions of n_{H} and n_{L}.

In grating couplers, the grating diffraction is governed by the phase matching condition [19]:

$$k_0 \cdot n_{\text{eff}} = k_0 \cdot n_c \cdot sin(\theta) + m \cdot \frac{2\pi}{\Lambda} \quad \textbf{(1)}$$

where $k_0 = \frac{2\pi}{\lambda}$, n_{eff} is the effective index of the grating, n_c is the refractive index of the cladding, θ is the incident angle in free space, Λ is the grating period, and m is an integer denoting the diffraction order (here m=1). Similar to [13], we estimate the 1-dB bandwidth of a grating coupler using the wavelength dependent diffraction angle:

$$\Delta\lambda_{1\text{dB}} = \Delta\theta_{1\text{dB}} \cdot 2|\frac{d\lambda}{d\theta}| = \Delta\theta_{1\text{dB}} \cdot 2|\frac{-n_c \cdot cos(\theta)}{\frac{1}{\Lambda} - \frac{dn_{\text{eff}}}{d\lambda}}| \quad \textbf{(2)}$$

where $\Delta\theta_{1\text{dB}}$ is a constant that depends solely on the fiber parameters and the calculated results match well with the measurement when $\Delta\theta_{1\text{dB}}$ equals 0.047. $|\frac{d\lambda}{d\theta}|$ can be obtained from Eq. (1) and the factor of 2 accounts for the 1-dB bandwidth including the wavelength range both above and below the central operating wavelength. From Eq. (1), we can express the grating period as:

$$\Lambda = \frac{\lambda}{n_{\text{eff}} - n_c \cdot sin(\theta)} \quad \textbf{(3)}$$

We also know that the group index of the grating, n_g, is defined as [19] :

$$n_g = n_{\text{eff}} - \lambda\frac{dn_{\text{eff}}}{d\lambda} \quad \textbf{(4)}$$

Using Eqs.(2) - (4), the 1-dB bandwidth becomes:

$$\Delta\lambda_{1\text{dB}} = \Delta\theta_{1\text{dB}} \cdot 2|\frac{-n_c \cdot cos(\theta) \cdot \lambda}{n_g - n_c \cdot sin(\theta)}| \quad \textbf{(5)}$$

Given that $\Delta\theta_{1\text{dB}}$ and n_c are constants, we can see that the bandwidth is only dependent on the group index and the incident angle for a given λ. Equation (5) shows us that the 1-dB bandwidth of a grating coupler can be increased by reducing the group index of the grating. For a given group index, an optimal incident angle, that gives the largest bandwidth, can also be calculated using Eq.(5). The optimal incident angle, θ_{opt}, as a function of the group index of the grating is shown in Fig. 2, for values of n_g between 2.2 and 4.2; the simulated n_g for a unetched silicon waveguide is about 4.2, and the simulated n_g for a one-dimensional sub-wavelength grating with an overall fill factor of 0.2 is about 2.2. (where the material dispersion was not included in the calculation due to the fact that we used a constant refractive index for the estimation based on EMT). As mentioned above, if we wish to increase the bandwidth, a larger θ is required. Here, we chose $\theta = 25°$, which is the optimal incident angle for an n_g near the middle of the n_g range from 2.2 to 4.2.

As will become apparent from the discussion, the subsequent optimizations of our SWGC design parameters begins with the structure shown in Fig. 1(b). Our SWGCs are designed based on SOI wafers with 220 nm silicon and 3 µm buried silicon dioxide layers. Here, the grating of our SWGC is modelled as alternating regions of high and low refractive indices, where each grating period consists of a high index region with a refractive index of n_H and a low index region with a refractive index of n_L. The lengths of n_H and n_L are denoted as Λ_H and Λ_L. The length of the grating period is Λ, where $\Lambda = \Lambda_H + \Lambda_L$. The lengths of the sub-wavelength gratings in the high and the low index regions are denoted as l_H and l_L. The fill factor of the grating

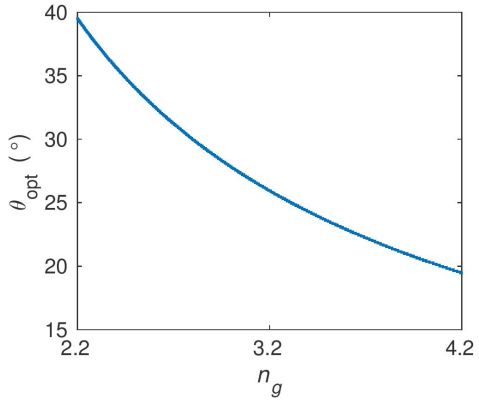

Fig. 2. Optimal incident angle, θ_{opt}, as a function of the group index of a grating coupler, n_g.

coupler, denoted as ff, is defined as the ratio of Λ_H to Λ. The numbers of gratings in each high and low index region are N_H and N_L, respectively. The fill factors of the high and low index regions, denoted as ff_H and ff_L, are defined as $N_H * l_H/\Lambda_H$ and $N_L * l_L/\Lambda_L$, respectively.

The two-dimensional finite-difference time-domain (FDTD) method was used to optimize the design parameters of our SWGCs. A figure of merit (FOM), defined as the product of the 1-dB bandwidth and the coupling efficiency (CE) , was used to predict the performance of an SWGC. Having chosen $\theta = 25°$, we have completed the first step in our design methodology. We now optimize our SWGC design in three more steps. In the second step, we optimized four design parameters, Λ, ff , n_H, and n_L, to achieve the maximum FOM using the PSA in FDTD Solutions (an FDTD-method Maxwell equation solver from Lumerical Solutions, Inc.). The design parameters, with the largest FOM for θ =25° are shown in row 2 of Table 1. In the third step, using our optimized n_H and n_L from the second step, ff_H and ff_L were calculated using zeroth-order EMT [18, 20]. The dimensions of the sub-wavelength grating have both a lower limit, which comes from the fabrication limitations, and an upper limit, which is determined using EMT. Since the calculated ff_L and ff_H are only approximations, further optimizations with boundary conditions were done using the PSA, as before, with the optimized values shown in row 3 of Table 1. Finally, we determined the number of sub-wavelength gratings in the high and low index regions, *i.e.*, N_H and N_L. The dimensions of the sub-wavelength gratings should be small enough to allow EMT to work and large enough to be fabricated. Based on the optimized values of ff_H and ff_L, we simulated the allowed combinations of N_H and N_L, and have given the optimized values in the last row of Table 1.

Table 1. Optimization Steps and Design Parameters

Step 1:	$\theta = 25°$			
Step 2:	Λ =1130 nm	ff =0.5	n_H = 2.78	n_L = 1.8
Step 3:	ff_H=0.49	ff_L = 0.13		
Step 4:	N_H= 3	N_L=2		

The simulated transmission and reflection spectra of the optimized SWGC, having the parameters given in Table 1, are shown in Fig. 3(a). Since all of the design optimizations were done using 2D FDTD simulations, we then verified the designs using

3D simulations. The simulated transmission spectra for both the 2D and the 3D simulations are shown in Fig. 3(a). The simulated reflection spectra of the straight and focusing SWGCs are also shown in Fig. 3(a). As compared to the straight SWGC, the back reflection from the focusing SWGC is smaller, which means that the focusing design not only reduces the footprint, but also suppresses the back reflection. The SWGC has an CE of -3.6 dB and a 1-dB bandwidth of 84 nm. The FOM that we defined takes both the bandwidth and CE into consideration, the result being that the SWGC with the largest FOM may not necessarily have the largest bandwidth. Based on the design parameters in Table 1, we simulated the 1-dB bandwidths and the peak CEs as we varied ff_L. As we varied ff_L, ff_H was also varied such that the operating wavelength of the grating coupler remained constant. Fig. 3(b) shows the simulated 1-dB bandwidth and peak CE as a function of ff_L. We can see that the bandwidth of the grating coupler is inversely proportional to ff_L, and that broader bandwidths can be achieved with smaller ff_Ls. However, the minimum ff_L is determined by the minimum feature size provided by the fabrication facility.

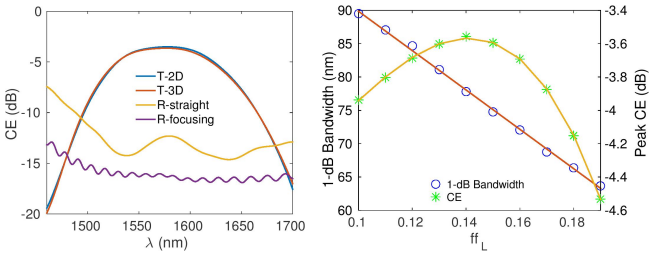

Fig. 3. (a) Simulated transmission and reflection spectra of the SWGC with the design parameters shown in Table 1; (b) simulated 1-dB bandwidth and peak CE as a function of ff_L.

Test structures, consisting of an input SWGC and an output SWGC, connected by a strip waveguide, were fabricated using electron beam lithography at the University of Washington [21]. Since it is known that focusing SWGCs are more space-efficient than straight SWGCs, both types were fabricated for comparison purposes. The purpose of comparing them is to determine which has the higher FOM and, also, to confirm whether the focusing SWGC has a lower back reflection than the straight SWGC. The straight SWGCs were 12 µm wide and in order to keep the total device length to a reasonable number, we used 150 µm long tapers to couple the light from the grating to the 500 nm wide waveguide. The focusing SWGCs were generated using the method demonstrated in [11, 22]. Scanning electron microscope (SEM) images of the as-fabricated straight and focusing SWGCs are shown in Fig. 4.

Based on the simulation results shown in Fig. 3(b), design variations were fabricated as shown in Table 2. The fabricated devices were measured using our fiber-array-based automated measurement setup, the fiber array was polished at 24.7° to accommodate the required incident angles. Figure 5 shows the measured transmission spectra of the focusing and straight SWGCs with ff_L=0.1 and ff_H=0.52. The simulated transmission spectrum, using the same grating design as the measured device, is shown in the same figure. The measured focusing and straight SWGCs, have maximum CEs of -5.5 dB and -5.8 dB, respectively. Both have 1-dB bandwidths of 90 nm, with central wavelengths of about 1578 nm.

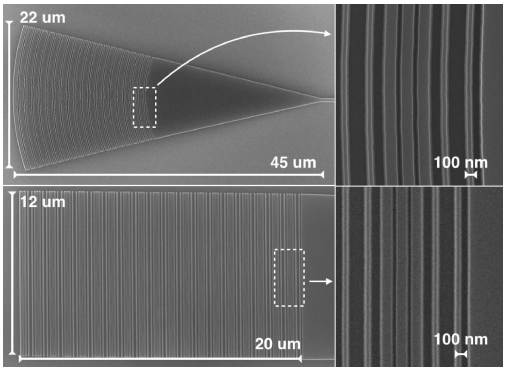

Fig. 4. SEM images of the as-fabricated focusing and straight SWGCs. (For the straight SWGC, the taper is not shown.)

Table 2. Design Variations

Focusing Grating	ff_L:	0.1 - 0.19	ff_H :	0.52 - 0.43
Straight Grating	ff_L:	0.1 - 0.18	ff_H:	0.52 - 0.44

The CE of the straight SWGC is higher than that of the focusing one because we used a short linear taper in it. The length of the linear tapers used in our straight SWGC were 150 µm, which is not long enough to allow adiabatic coupling between the grating and the waveguide. It should be noted that the oscillation ripples in the spectrum of the focusing SWGC are smaller than those in the spectrum of the straight SWGC, which confirms that the focusing design not only reduces the footprint of the device, but also suppresses the back reflection from the grating. The extinction ratios (ERs) of the ripples near the central wavelength of the focusing SWGC are about 0.08 dB, which correspond to back reflections of less than -23 dB, whereas the ERs of the ripples near the central wavelength of the straight SWGC are about 0.2 dB, which correspond to back reflections of less than -19 dB. In addition, the back reflection of the focusing SWGCs are more consistent over the 1-dB bandwidth wavelength range, while the back reflection of the straight SWGCs increases gradually as the wavelength decreases, which matches the simulation results shown in Fig. 3(a).

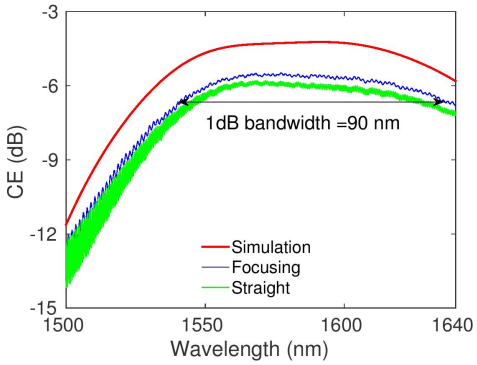

Fig. 5. Transmission spectra of the simulated SWGC (red), the measured focusing SWGC (blue), and the measured straight SWGC (green).

Figure 6 shows the measured 1-dB bandwidths and CEs of the fabricated focusing and straight SWGCs with the design

variations shown in Table 2. For the focusing SWGCs, as ff_L changed from 0.1 to 0.19, the 1-dB bandwidths changed from 90 nm to 48 nm and the CEs varied between -5.5 dB and -3.8 dB. For the straight SWGCs, as ff_L changed from 0.1 to 0.18, the 1-dB bandwidths changed from 90 nm to 48 nm and the CEs varied between -5.8 dB and -4.2 dB. The measured 1-dB bandwidths of both focusing and straight SWGCs follow the same trend as shown in Fig. 3(b) except that the slope of the measured 1-dB bandwidth variations were slightly larger than those of the simulations. The increased slope may result from the fact that the $\Delta\theta_{1dB}$ of the fiber model that we used in the simulations is smaller than the $\Delta\theta_{1dB}$ of the fibers that we used in the measurements. The measured CEs of the focusing and straight SWGCs are lower than the simulated results, which may come from several sources, such as the measurement system, fabrication errors, *etc.* In addition, the measured peak CE corresponds to a larger ff_L than was used in the simulation, which may come from the fact that the ff_Ls of the fabricated devices were smaller than the design values.

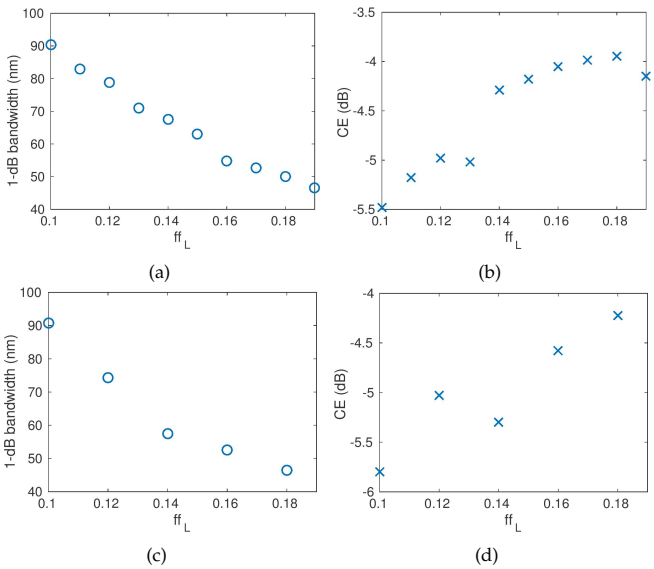

Fig. 6. Measured (a) 1-dB bandwidths and (b) CEs of the fabricated focusing SWGCs with ff_L ranging from 0.1 to 0.19; measured (c) 1-dB bandwidths and (d) CEs of the fabricated straight SWGCs with ff_L ranging from 0.1 to 0.18.

We presented a methodology to design broadband SWGCs using one dimensional sub-wavelength gratings. Both straight SWGCs and focusing SWGCs with 1-dB bandwidths of 90 nm were designed and fabricated. Back reflections from the SWGCs were suppressed by using focusing sub-wavelength grating designs, and a measured back reflection below -23 dB was achieved, which is comparable to state-of-the-art shallow etched grating couplers [23].

FUNDING INFORMATION

Natural Sciences and Engineering Research Council of Canada (NSERC).

ACKNOWLEDGMENTS

The devices were fabricated by the Washington Nanofabrication Facility (WNF) at the University of Washington, part of the National Science Foundation National Nanotechnology Infrastructure Network (NNIN). We acknowledge CMC, Lumerical Solutions, Inc., and Mentor Graphics for the design software.

REFERENCES

1. L. Chrostowski and M. Hochberg, (Cambridge University Press, 2015).
2. S. McNab, N. Moll, and Y. Vlasov, Opt. Express **11**, 2927–2939 (2003).
3. A. Mekis, S. Gloeckner, G. Masini, A. Narasimha, T. Pinguet, S. Sahni, and P. De Dobbelaere, JSTQE, IEEE **17**, 597–608 (2011).
4. D. Vermeulen, S. Selvaraja, P. Verheyen, G. Lepage, W. Bogaerts, P. Absil, D. Van Thourhout, and G. Roelkens, Opt. Express **18**, 18278–18283 (2010).
5. R. Halir, P. Cheben, J. Schmid, R. Ma, D. Bedard, S. Janz, D.-X. Xu, A. Densmore, J. Lapointe, and I. Molina-Fernández, Opt. Lett. **35**, 3243–3245 (2010).
6. N. Na, H. Frish, I.-W. Hsieh, O. Harel, R. George, A. Barkai, and H. Rong, Opt. Lett. **36**, 2101–2103 (2011).
7. A. Mekis, S. Abdalla, P. M. De Dobbelaere, D. Foltz, S. Gloeckner, S. Hovey, S. Jackson, Y. Liang, M. Mack, G. Masini et al., in "SPIE OPTO," (International Society for Optics and Photonics, 2012), pp. 82650A–82650A.
8. Y. Ding, C. Peucheret, H. Ou, and K. Yvind, Opt. Lett. **39**, 5348–5350 (2014).
9. W. S. Zaoui, A. Kunze, W. Vogel, M. Berroth, J. Butschke, F. Letzkus, and J. Burghartz, Opt. Express **22**, 1277–1286 (2014).
10. Y. Wang, X. Wang, J. Flueckiger, H. Yun, W. Shi, R. Bojko, N. A. F. Jaeger, and L. Chrostowski, Opt. Express **22**, 20652–20662 (2014).
11. Y. Wang, H. Yun, Z. Lu, R. Bojko, W. Shi, X. Wang, J. Flueckiger, F. Zhang, M. Caverley, N. A. F. Jaeger, and Lukas Chrostowski, IEEE Photon. J. **7**, (2015).
12. Z. Xiao, F. Luan, T.-Y. Liow, J. Zhang, and P. Shum, Opt. Lett. **37**, 530–532 (2012).
13. X. Chen, K. Xu, Z. Cheng, C. K. Fung, and H. K. Tsang, Opt. Lett. **37**, 3483–3485 (2012).
14. Z. Xiao, T.-Y. Liow, J. Zhang, P. Shum, and F. Luan, Opt. Express **21**, 5688–5700 (2013).
15. X. Xu, H. Subbaraman, J. Covey, D. Kwong, A. Hosseini, and R. T. Chen, Opt. Lett. **38**, 3588–3591 (2013).
16. Q. Zhong, V. Veerasubramanian, Y. Wang, W. Shi, D. Patel, S. Ghosh, A. Samani, L. Chrostowski, R. Bojko, and D. V. Plant, Opt. Express **22**, 18224–18231 (2014).
17. J. Robinson and Y. Rahmat-Samii, Antennas and Propagation, IEEE Transactions on **52**, 397–407 (2004).
18. C. W. Haggans, R. K. Kostuk, and L. Li, JOSA A **10**, 2217–2225 (1993).
19. P. Yeh and A. Yariv, (Oxford University Press, 2007).
20. X. Chen and H. K. Tsang, Opt. Lett. **36**, 796–798 (2011).
21. R. J. Bojko, J. Li, L. He, T. Baehr-Jones, M. Hochberg, and Y. Aida, J. Vac. Sci. Technol. B **29**, 06F309 (2011).
22. F. Van Laere, T. Claes, J. Schrauwen, S. Scheerlinck, W. Bogaerts, D. Taillaert, L. O. Faolain, D. Van Thourhout, and R. Baets, IEEE Photon. Technol. Lett. **19**, 1919–1921 (2007).
23. D. Vermeulen, Y. De Koninck, Y. Li, E. Lambert, W. Bogaerts, R. Baets, and G. Roelkens, Opt. Express **20**, 22278–22283 (2012).

REFERENCES

1. L. Chrostowski and M. Hochberg, Silicon Photonics Design: From Devices to Systems (Cambridge University Press, 2015).
2. S. McNab, N. Moll, and Y. Vlasov, "Ultra-low loss photonic integrated circuit with membrane-type photonic crystal waveguides," Opt. Express **11**, 2927–2939 (2003).
3. A. Mekis, S. Gloeckner, G. Masini, A. Narasimha, T. Pinguet, S. Sahni, and P. De Dobbelaere, "A grating-coupler-enabled cmos photonics platform," JSTQE, IEEE **17**, 597–608 (2011).
4. D. Vermeulen, S. Selvaraja, P. Verheyen, G. Lepage, W. Bogaerts, P. Absil, D. Van Thourhout, and G. Roelkens, "High-efficiency fiber-to-chip grating couplers realized using an advanced CMOS-compatible silicon-on-insulator platform," Opt. Express **18**, 18278–18283 (2010).
5. R. Halir, P. Cheben, J. Schmid, R. Ma, D. Bedard, S. Janz, D.-X. Xu, A. Densmore, J. Lapointe, and I. Molina-Fernández, "Continuously apodized fiber-to-chip surface grating coupler with refractive index engineered subwavelength structure," Opt. Lett. **35**, 3243–3245 (2010).
6. N. Na, H. Frish, I.-W. Hsieh, O. Harel, R. George, A. Barkai, and H. Rong, "Efficient broadband silicon-on-insulator grating coupler with low backreflection," Opt. Lett. **36**, 2101–2103 (2011).
7. A. Mekis, S. Abdalla, P. M. De Dobbelaere, D. Foltz, S. Gloeckner, S. Hovey, S. Jackson, Y. Liang, M. Mack, G. Masini et al., "Scaling CMOS photonics transceivers beyond 100 Gb/s," in "SPIE OPTO," (International Society for Optics and Photonics, 2012), pp. 82650A–82650A.
8. Y. Ding, C. Peucheret, H. Ou, and K. Yvind, "Fully etched apodized grating coupler on the SOI platform with -0.58 dB coupling efficiency," Opt. Lett. **39**, 5348–5350 (2014).
9. W. S. Zaoui, A. Kunze, W. Vogel, M. Berroth, J. Butschke, F. Letzkus, and J. Burghartz, "Bridging the gap between optical fibers and silicon photonic integrated circuits," Opt. Express **22**, 1277–1286 (2014).
10. Y. Wang, X. Wang, J. Flueckiger, H. Yun, W. Shi, R. Bojko, N. A. F. Jaeger, and L. Chrostowski, "Focusing sub-wavelength grating couplers with low back reflections for rapid prototyping of silicon photonic circuits," Opt. Express **22**, 20652–20662 (2014).
11. Y. Wang, H. Yun, Z. Lu, R. Bojko, W. Shi, X. Wang, J. Flueckiger, F. Zhang, M. Caverley, N. A. F. Jaeger, and Lukas Chrostowski, "Apodized focusing fully etched sub-wavelength grating couplers," IEEE Photon. J. **7**, (2015).
12. Z. Xiao, F. Luan, T.-Y. Liow, J. Zhang, and P. Shum, "Design for broadband high-efficiency grating couplers," Opt. Lett. **37**, 530–532 (2012).
13. X. Chen, K. Xu, Z. Cheng, C. K. Fung, and H. K. Tsang, "Wideband subwavelength gratings for coupling between silicon-on-insulator waveguides and optical fibers," Opt. Lett. **37**, 3483–3485 (2012).
14. Z. Xiao, T.-Y. Liow, J. Zhang, P. Shum, and F. Luan, "Bandwidth analysis of waveguide grating coupler," Opt. Express **21**, 5688–5700 (2013).
15. X. Xu, H. Subbaraman, J. Covey, D. Kwong, A. Hosseini, and R. T. Chen, "Colorless grating couplers realized by interleaving dispersion engineered subwavelength structures," Opt. Lett. **38**, 3588–3591 (2013).
16. Q. Zhong, V. Veerasubramanian, Y. Wang, W. Shi, D. Patel, S. Ghosh, A. Samani, L. Chrostowski, R. Bojko, and D. V. Plant, "Focusing-curved subwavelength grating couplers for ultra-broadband silicon photonics optical interfaces," Opt. Express **22**, 18224–18231 (2014).
17. J. Robinson and Y. Rahmat-Samii, "Particle swarm optimization in electromagnetics," Antennas and Propagation, IEEE Transactions on **52**, 397–407 (2004).
18. C. W. Haggans, R. K. Kostuk, and L. Li, "Effective-medium theory of zeroth-order lamellar gratings in conical mountings," JOSA A **10**, 2217–2225 (1993).
19. P. Yeh and A. Yariv, Photonics: Optical electronics in modern communication (Oxford University Press, 2007).
20. X. Chen and H. K. Tsang, "Polarization-independent grating couplers for silicon-on-insulator nanophotonic waveguides," Opt. Lett. **36**, 796–798 (2011).
21. R. J. Bojko, J. Li, L. He, T. Baehr-Jones, M. Hochberg, and Y. Aida, "Electron beam lithography writing strategies for low loss, high confinement silicon optical waveguides," J. Vac. Sci. Technol. B **29**, 06F309 (2011).
22. F. Van Laere, T. Claes, J. Schrauwen, S. Scheerlinck, W. Bogaerts, D. Taillaert, L. O. Faolain, D. Van Thourhout, and R. Baets, "Compact focusing grating couplers for silicon-on-insulator integrated circuits," IEEE Photon. Technol. Lett. **19**, 1919–1921 (2007).
23. D. Vermeulen, Y. De Koninck, Y. Li, E. Lambert, W. Bogaerts, R. Baets, and G. Roelkens, "Reflectionless grating couplers for silicon-on-insulator photonic integrated circuits," Opt. Express **20**, 22278–22283 (2012).